Blending of Newtonian and Shear-Thinning Fluids

in a Tank Stirred with a Helical Screw Agitator

JOËLLE AUBIN, ISABELLE NAUDE, JOËL BERTRAND and CATHERINE XUEREB*

ABSTRACT

Newtonian and non-Newtonian laminar fluid flow has been simulated using Computational Fluid Dynamics for a cylindrical vessel stirred by a helical screw agitator. Simulations have been performed for a vessel geometry with and without a draft tube. Simulated flow patterns in the vessel have been examined and compared with the experimental work of previous authors. The power number and the circulation number have been evaluated, and interpreted in a similar manner to other works. The P_O.Re constant, A, has been determined to be 295 for the geometry with the draft tube and 150 for that without the draft tube. These results are in the same range as previously reported values. The Metzner and Otto constant, k, has been evaluated to be 16.23 which is in excellent agreement with experimental results reported in the literature.

Keywords: CFD, screw agitator, non-Newtonian, power consumption, draft tube

INTRODUCTION

Industrial utilisation of Computational Fluid Dynamics (CFD) has experienced phenomenal advances since the early 1980s, which has resulted in increased interest in the analysis of fluid flow in stirred tanks by means of numerical simulation. The majority of published work in the domain of CFD and stirred vessels involves studies of classical agitators such as the Rushton turbine[1-5] and the pitched blade turbine[6,7] in the turbulent flow regime. CFD mixing studies in the laminar flow regime are more rare and have been restricted to simple geometries[8]. Development of unstructured and hybrid meshing techniques has allowed the representation of more complicated geometries[9], as are often found in laminar flow mixing. The helical screw impeller is a major type of agitator used in creeping laminar flow mixing in industrial processes. For the mixing of highly viscous liquids, the screw agitator centred in a draft tube producing axial flow has been found to be highly efficient[10,11]. Since the late 1960's, the hydrodynamic characteristics, power consumption and circulation capacities of close clearance agitators such as the helical screw, have been extensively studied[10-23]. These studies however have focused on experimental measures using pilot-size vessels. To our knowledge, there have been no published papers on the CFD simulation of helical screw impellers. This means, that until now, only global values in the vessel have been known. In fact, there are not a lot of experimental techniques are available for the local hydrodynamic characterisation of high viscosity fluids. The classic techniques, such as Laser Doppler Velocimetry (LDV) and Particle Image Velocimetry (PIV), which allow local

measurements using a penetrating laser beam are limited in such high viscosity fluids due to light diffusion.

The purpose of this work is to demonstrate the benefit of a draft tube for effectively mixing viscous and complex fluids in a screw-agitated vessel using CFD simulations. In addition, it provides a solution for the determination of local values in such installations that cannot be obtained experimentally due to inherent difficulties. This paper presents the CFD simulation results for laminar Newtonian and non-Newtonian liquid flow in a cylindrical tank with and without draft tube, stirred by a centred screw agitator. The effects of the vessel geometry, fluid rheology and the Reynolds number on the hydrodynamics have been investigated. Power consumption characteristics of the impeller in different vessel geometries as well as several fluids have also been studied. The simulated results have been compared with the global experimental data available. Comparisons with local experimental data are limited due to the lack of data available.

THEORY

Power consumption

In the laminar flow regime, the power consumption of an agitator may be calculated by integration of the viscous dissipation over the entire volume of fluid in the vessel. This may be represented by the following volume integral :

$$P = -\iiint (\tau : \nabla \upsilon).dV \tag{1}$$

Newton's viscosity law for an incompressible fluid states that the shear stress τ is proportional to the 'rate of deformation tensor' or the shear rate Δ, with Cartesian co-ordinates $\Delta_{ij} = (\delta v_i / \delta x_j) + (\delta v_j / \delta x_i)$:

$$\tau = -\mu \Delta \tag{2}$$

For non-Newtonian fluids, the viscosity becomes the apparent viscosity μ_a, a scalar and is a function of Δ, as well as pressure and temperature.

For non-Newtonian shear thinning fluids, shear stress may be described by the *Ostwald-de Waele* model :

$$\tau = -m \left| \frac{1}{2} \Delta : \Delta \right|^{\frac{n-1}{2}} . \Delta \tag{3}$$

These equations lead to the following equation for the power consumption:

$$P = \iiint m \left| \Phi_v \right|^{\frac{n-1}{2}} . \Phi_v \, dV \tag{4}$$

where

$$\Phi_v = 2\left[\left(\frac{\partial v_r}{\partial r}\right)^2 + \left(\frac{\partial v_\theta}{\partial \theta}\right)^2 + \left(\frac{\partial v_z}{\partial z}\right)^2 \right] + \left(\frac{\partial v_r}{\partial \theta} + \frac{\partial v_\theta}{\partial r}\right)^2 + \left(\frac{\partial v_r}{\partial z} + \frac{\partial v_z}{\partial r}\right)^2 + \left(\frac{\partial v_\theta}{\partial z} + \frac{\partial v_z}{\partial \theta}\right)^2$$

The dimensionless power number may be expressed by equation 5.

$$P_O = \frac{P}{\rho N^3 d^5} \tag{5}$$

Power number - Reynolds number relationship and the Metzner and Otto constant

In the creeping flow regime, the typical 'power curve' (i.e. Po *versus* Re) for Newtonian fluids shows that the power number is inversely proportional to the Reynolds number. This can be expressed by the relation:

$$P_O . Re = \frac{P}{\mu N^2 d^3} = A \tag{6}$$

where A is a constant, being a function of the agitator type and the system geometry only.

For non-Newtonian fluids however, the Reynolds number is a function of the apparent viscosity μ_a (and thus the flow behaviour index, n, and the consistency index, m), in the case where the rheological behaviour of the fluid can be correctly represented by a power law. Metzner and Otto (1957) characterised the fluid motion in the impeller region by an average shear rate which is linearly related to the rotational speed of the impeller:

$$\bar{\gamma} = kN \tag{7}$$

k is Metzner and Otto constant which is characteristic for a given type of agitator and system geometry. Substituting this relation into a simple power law (equation 3) gives the apparent Reynolds number, Re_a:

$$Re_a = \frac{Re_g}{k^{n-1}} \tag{8}$$

where Re_g is the generalised Reynolds number given by equation 9:

$$Re_g = \frac{\rho N^{(2-n)} d^2}{m} \tag{9}$$

The generalised power relation, similar to equation 6, may be expressed as:

$$P_O . Re_a = A \tag{10}$$

Circulation Number

The global circulation rate Q_c, is the flow rate driven by the circulation loop which is created by the impeller. It may be determined by integrating the axial velocity at a horizontal plane corresponding to the circulation centre. The non-dimensional circulation number N_{Qc} is calculated in a similar manner to the pumping number:

$$N_{Qc} = \frac{Q_c}{Nd^3} \tag{11}$$

INVESTGATED SYSTEM

The helical screw agitator is centred in a flat-bottomed cylindrical tank with diameter D=0.634m, and a liquid height, H=D. The diameter of the agitator is defined as a fraction of the tank diameter, d=0.64D, with a period equal to the diameter s=d. The draft tube has a diameter of d_t=1.1D. Other geometrical parameters of the vessel are summarised in Table 1 and the schematic diagram is shown in Figure 1. CFD simulations have been performed for solutions of glucose, Carbopol-940 and Natrosol (hydroxy ethyl cellulose). The rheological properties for the simulated liquids have been taken from the literature[13,14] and are given in Table 2. The operating conditions for each simulation are tabulated in Table 3.

CFD METHOD

The commercial CFD package FLUENT 5 was used to simulate the flow induced by the helical screw agitator. The configuration is represented 3-dimensionally using an unstructured tetrahedral mesh and the geometry of the impeller is shown in Figure 2.

The CFD code was used to solve in Cartesian co-ordinates, the continuity and momentum equations for the laminar flow of Newtonian and non-Newtonian fluids. Resolution of the algebraic equations was carried out using the Semi-Implicit algorithm Pressure Linked Equation (SIMPLE) with a second order upwind discretisation scheme. The computations were performed on a Silicon Graphics ORIGIN 200 computer with a 225 MHz R10000 processor.

The vessel walls and bottom have been modelled with a no-slip boundary condition. The free liquid surface has been modelled with a no stress condition applied, and the draft tube and helical part of the agitator have been modelled with a zero thickness. The absence of baffles, and thus of rotor-stator interactions, has allowed the use of the rotating reference frame technique to simulate the entire non-symmetrical geometry.

RESULTS AND DISCUSSION

Effect of grid size

To investigate the effect of grid size, the laminar flow of a Newtonian fluid has been solved using three mesh sizes, the first comprising 122027 cells, the second consisting of 92960 cells with local refinement near the impeller and the third containing 43631 cells. Local refinement has been tested because the effect of grid size will be most noticeable where sharp gradients in the flow field exist, i.e. in the impeller region, (Ranade and Joshi (1990), Naude et al. (1998)). The radial profiles of the axial velocity, taken at $z = 2/5H$ between the shaft and the draft tube and along a line where the helical part of the impeller does not obstruct the flow, are shown in Figure 3. It can be seen that there is little difference between the results of the three grids. In Figures 9, 10 and 11, the effect of grid size has been evaluated with P_0 (equation (5)). Again, there is minimal difference in the results. For computing facility, the grid of 43631 cells has been retained for all other simulations.

Effect of the geometrical configuration on hydrodynamics

The effect of the geometry on the hydrodynamics of the vessel has been investigated, Figures 4, 5 and 6. The flow of a Newtonian fluid in the vessel with draft tube has been compared to the flow in the vessel without draft tube. Results for non-Newtonian flow without draft tube are not reported here due to the extremely inefficient circulation observed. The simulation numbers correspond to the operating conditions given in Table 3.

Velocity flow patterns for the screw agitated vessel with and without draft tube are shown in Figure 4. In Figure 4(a), when the geometry does not include a draft tube, the Newtonian fluid is projected in a radial direction away from the impeller with some axial movement. Due to the absence of the draft tube, the radial flow generated by the impeller edge, continues in a radial direction towards the vessel wall. The flow is then reoriented in an upwards direction due to the presence of the vessel wall and by other upward moving fluid. This causes the formation of self-feeding zones at the impeller edge. This phenomenon is even more pronounced when mixing non-Newtonian fluids, characterising inefficient fluid circulation. In Figure 4(b), a dominant axial circulation is observed. The screw pushes the fluid downwards in the draft tube with a simultaneous strong radial component at the outer edge of the impeller. The presence of the vessel bottom induces a change in direction of the fluid motion and the fluid is pumped upwards in the annular region between the draft tube and the vessel wall. A circulation loop is formed as the liquid is pushed down once again, into the draft tube. For the non-Newtonian liquid with draft tube, Figure 4(c), the velocity flow patterns are identical to those observed in the same vessel mixing a Newtonian liquid.

Figure 5 shows the velocity flow patterns obtained at 2/5H for the three configurations. When the draft tube is not present, Figure 5(a), a strong tangential flow is present almost everywhere in the horizontal section and there is no obvious division between the axial and tangential velocity components. In Figures 5(b) and 5(c), a strong tangential fluid motion is observed within the draft tube, being strongest at the impeller edge. In the annular region between the draft tube and the vessel wall, the tangential and radial velocity components are non-existent. In Figure 4, a strong axial flow was observed in this region of the vessel.

Figure 6 shows the velocity flow patterns in two different horizontal planes. The first, just below the liquid surface and the second, just above the vessel bottom. At the top of the vessel without the draft tube, Figure 6(a-i), the flow just below the liquid surface is strongly tangential and there appears to be no movement towards the centre of the vessel. On the other hand, when the draft tube is present Figures 6(b-i) and 6(c-i), fluid flow is directed towards the agitator in the centre, from the vessel walls. Just above the vessel base without the draft tube, the flow at the bottom is predominantly tangential with only slight deviations towards the vessel wall. In the two cases with the draft tube, the flow is composed of tangential and radial components which direct outwards towards the side wall. However, there exists an important tangential motion at the edge of the agitator blade for both vessel geometries, Newtonian and non-Newtonian flow.

Effects of the fluid rheology and the Reynolds number on axial velocity profiles

The effects of the liquid rheology and the Reynolds number, on the axial velocity profiles in the annular region between the draft tube and the vessel wall at 2/5H, are shown in Figures 7 and 8. The dimensionless axial velocity profiles appear to 'flatten out' with a decrease in the flow behaviour index, n. This corresponds to classical pipe flows and Caussanel (1990) has reported similar experimental observations. Figure 7 also shows that the simulated dimensionless axial velocity for a particular fluid is independent of the Reynolds number. This phenomenon has also been reported by Caussanel (1990).

A comparison of simulated results of the dimensionless axial velocity with experimental results found by Caussanel (1990) is made in Figure 8. The experimental measurements of the axial velocity, taken with hot film anemometry[13], show little dependence on the flow behaviour index, n. The simulated results show a stronger dependence on the index n. The incoherence of these results may be explained by the known inaccuracy of hot film anemometry for the measurement of very small velocities, as well as the difficulties encountered when trying to calibrate the probe with a fluid that must have the same local rheological properties as the fluid in the vessel.

Power consumption

To demonstrate the dependence of the constant A on the vessel geometry, the power number as a function of the Reynolds or apparent Reynolds number has been plotted on a logarithmic scale, Figure 9. A straight line correlation according to a logarithmic form of equation 10 gives A to equal 295 for the geometry with draft tube and 150 for the geometry with draft tube. A summary of values for A reported in the literature are given in Tables 4 and 5. The values reported here for both geometries are in the range of those noted in the literature. Slight differences in the reported values of A and variations of geometric ratios between authors must be considered, since small changes in vessel geometry can result in substantial changes in power consumption[19].

The logarithmic plot of the power number as a function of the Reynolds number, Re_g, in the laminar region studied is shown in Figure 10. For constant values of the flow behaviour index, n, the plot is a straight line with a gradient –1. These results are in excellent agreement with the experimental results presented in the literature[19].

A semi-logarithmic plot of $P_O.Re_g$ *versus* (1-n) is plotted in Figure 11 in order to demonstrate the Metzner and Otto method[12]. A straight line correlates the data giving the Metzner and Otto constant, k, equal to 16.23 with a correlation coefficient, $r^2 = 0.9973$. Values of k found by other authors are given in Table 6. The CFD result obtained in this work is in excellent agreement with the experimental value found by Rieger and Novak (1973). The large difference in the value of k found in this work and with that of Prokopec and Ulbrecht (1970) may by explained by the smaller d_t/d ratio and different length screw used by the experimental prediction[19].

The dependence of the circulation number on the Reynolds number is presented in Figure 12. This graph shows that the circulation number is independent of Reynolds number in the laminar flow regime studied. This phenomenon agrees with the previously reported works[11,14,21,22]. As the circulation number is a function of geometry only[21], the dependence of the circulation number on the geometry is verified by comparing the values for the Newtonian system with a draft tube and that without. Without the draft tube, the circulation number is remarkably smaller than for the system with a draft tube, corresponding to the high circulation efficiency of the screw agitator with a draft tube. A reduction in

the circulation number with a decrease in the flow behaviour index, n, has also been observed. This same behaviour has been reported in literature[14,22] and has been explained by the damping of axial flow due to elastic anomalies of the liquid[14].

CONCLUSIONS

A numerical approach has been taken to investigate the mixing characteristics of Newtonian and non-Newtonian laminar fluid flow in a screw agitated vessel using a commercial unstructured CFD code. It has been demonstrated with simulated velocity flow patterns, that geometrical vessel configuration with draft tube is more efficient in terms of circulation, as flow is uniformly pushed downwards in the draft tube and carried upwards in the annular region close to the vessel wall. The axial velocity, between the draft tube and the vessel wall, has shown to be more significant for a Newtonian liquid than a shear-thinning non-Newtonian liquid. In this area, the axial velocity is not influenced by the Reynolds number in the range of Reynolds studied. The constant Np.Re has been calculated from the simulated results and equals 150 for the vessel without draft tube and 295 for the vessel with draft tube. These values are in very good agreement with the experimental results of other authors. Simulated results have confirmed that P_O is inversely proportional to Re_g and is dependent on the flow behaviour index n. The Metzner and Otto constant, k, calculated using CFD equals 16.23 and has been validated with previous literature experimental values. Simulation results affirm that the circulation number is not influenced by the Reynolds number in a creeping laminar flow regime. The circulation number has been found to be influenced not only by the vessel geometry but also by elastic anomalies of the fluids. Overall, the investigation has shown that CFD can be a reliable method for the analysis of Newtonian and non-Newtonian laminar fluid flow in agitated tanks with complex geometries.

NOTATION

A	Constant (equation 6)	
c	Impeller off-bottom clearance (m)	
c_t	Draft tube top clearance (m)	
c_t'	Draft tube off-bottom clearance (m)	
D	Vessel diameter (m)	
d	Agitator diameter (m)	

d_a	Shaft diameter (m)
d_t	Draft tube diameter (m)
H	Liquid height (m)
k	Metzner and Otto constant
l_t	Draft tube length (m)
m	Consistency index ($kg.s^{n-2}.m^{-1}$)
n	Flow behaviour index
N	Rotational speed (rps)
N_{Qc}	Circulation number (dimensionless)
P_O	Power number (dimensionless)
P	Power consumption (W)
Q_c	Circulation flow rate ($m^3.s^{-1}$)
r	Radius (m)
R	Vessel radius (m)
Re	Reynolds number (dimensionless)
s	Period of helix (m)
v_r, v_θ, v_z	Velocity components in cylindrical co-ordinates ($m.s^{-1}$)
V	Vessel volume (m^3)
x, z	Cylindrical co-ordinates

Greek Symbols

Δ	Shear rate (s^{-1})
Φ_v	Viscous dissipation function (s^{-2})
$\bar{\dot{\gamma}}$	Average shear rate (s^{-1})
μ	Viscosity (Pa.s)
θ	Cylindrical co-ordinate
ρ	Density ($kg.m^{-3}$)
τ	Shear stress (Pa)
υ	Mass average velocity ($m.s^{-1}$)

Sub-scripts

        a   Apparent

        g   Generalised

REFERENCES

1. RANADE V.V. and JOSHI J.B., (1990), 'Flow Generated by a Disc Turbine: Part II. Mathematical Modelling and Comparison with Experimental Data', *Trans IChemE*, **68**, Part A, 34-50.

2. JAWORSKI Z., DYSTER K.N., MOORE I.P.T., NIENOW A.W. and WYZYNSKI M.L., (1997), 'The Use of Angle Resolved LDA Data to Compare Two Differential Turbulence Models Applied to Sliding Mesh CFD Flow Simulations in a Stirred Tank', *Récents Progrès en Génie des Procédés*, **11**, 51, 187-194.

3. LUO J.Y., GOSMAN A.D., ISSA R.I., MIDDLETON J.C. and FITZGERALD M.K., (1993), 'Full Flow Field Computation of Mixing in Baffled Stirred Vessels', *Trans IChemE*, **71**, Part A, 342-344.

4. LANE G.L. and KOH P.T.L., (1997), 'CFD Simulation of a Rushton Turbine in a Baffled Tank', *Proceedings of International Conference on CFD in Mineral and Metal Processing and Power Generation*, 377-385.

5. MICALE G., BRUCATO A., GRISAFI F. and CIOFALO M., (1999), 'Prediction of Flow Fields in a Dual-Impeller Stirred Vessel', *AIChE J.*, **45**, 3, 445-464.

6. RANADE V.V. and DOMMETI S.M.S., (1996), 'Computational Snapshot of Flow Generated by Axial Impellers in Baffled Stirred Vessels', *Trans IChemE*, **74**, Part A, 476-484.

7. HARVEY A.D. and ROGERS S.E., (1996), 'Steady and Unsteady Computation of Impeller-Stirred Reactors', *AIChE J.*, **42**, 10, 2701-2712.

8. LAMBERTO D.J., ALVAREZ M.M. and MUZZIO F.J., (1999), 'Experimental and Computational Investigation of the Laminar Flow Structure in a Stirred Tank', *Chem. Eng. Sci.*, **54**, 919-942.

9. NAUDE I., XUEREB C. and BERTRAND J., (1998), 'Direct Prediction of the Flows Induced by a Propeller in an Agitated Vessel Using an Unstructured Mesh', *Can. J. Chem. Eng.*, **76**, 631-640.

10. NOVAK V. and RIEGER F., 1969, 'Homogenization with Helical Screw Agitators', *Trans. IChemE*, **47**, T335-T340.

11. SEICHTER P, 1971, 'Efficiency of the Screw Mixers with a Draught Tube', *Trans. IChemE*, **49**, 117-123.

12. METZNER A.B. and OTTO R.E., 1957, 'Agitation of Non-Newtonian Fluids', *A.I.Ch.E. Journal*, **3**, 1, 3-10.

13. CAUSSANEL-LAURENT O., 1990, *Agitation Industrielle de Fluides Visqueux Newtoniens et Pseudoplastiques Approches Experimentale et Numerique*, Ph.D. Thesis, INPT, France.

14. CHAVAN V.V., FORD D.E. and ARUMUGAM M., 1975, 'Influence of Fluid Rheology on Circulation, Mixing and Blending', *Can. J. Chem. Eng.*, **53**, 628-635.

15. NOVAK V. and RIEGER F., 1977, 'Influence of Vessel to Screw Diameter Ratio on Efficiency of Screw Agitators', *Trans. IChemE,* **55**, 202-206.

16. SEICHTER P., DOHNAL J., and RIEGER F., 1981, 'Process Characteristics of Screw Impellers with a Draught Tube for Newtonian Liquids :The Power Input', *Collection Czechoslovak Chem. Commun.*, **46**, 2007-2020.

17. DEAK A., HAVAS G. and SAWINSKY J., 1985, 'The Power Requirements for Anchor, Ribbon and Helical-Screw Agitators', *Int. Chem. Eng.*, **25**, 3, 558-565.

18. HIROSE T. and MURAKAMI Y., 1986, 'Two-Dimensional Viscous Flow Model for Power Consumption in Close-Clearance Agitators', *J. Chem. Eng. Japan*, **19**, 6, , 568-574.

19. RIEGER F. and NOVAK V., 1973, 'Power Consumption of Agitators in Highly Viscous Non-Newtonian Liquids', *Trans. IChemE*, **51**, 105-111.

20. PROKOPEC L. and ULBRECHT J., 1970, 'Ruhrleistung eines Schraubenruhrere mit Leitrohr beim mischen nicht-Newtonschen Flussig keiten', *Chemie-Ingr-Tech.*, **42**, 530-534.

21. CHAVAN V.V. and ULBRECHT J., 1973, 'Internal Circulation in Vessels Agitated by Screw Impellers', *Chem. Eng. J.*, **6**, 213-223.

22. CARREAU P.J., PARIS J. and GUERIN P., 1992, 'Mixing of Newtonian and Non-Newtonian Liquids : Screw Agitator and Draft Coil System', *Can. J. Chem. Eng.*, **70**, 1071-1082.

23. GLUZ M.D. and PAVLUSHENKO I.S., 1967, 'Power consumption in agitation of non-Newtonian liquids', *J. Appl. Chem. USSR*, **40**, 7, 1430-1434.

D (m)	H/D	l_t/d	c_t/d	c_t'/d	d_t/d	d_a/D	d/D	s/d	c/d
0.634	1	1.3	0.13	0.13	1.1	0.18	0.64	1	0.06

Table 1

Test Liquid	Rheological Nature	Composition % wt	μ (Pa.s)	Flow Index n	Consistency Index m (kg.m^{-1}.s^{n-2})
Glucose Syrup[5]	Newtonian	65	1	-	-
Carbopol 940[5]	non-Newtonian	0.08	-	0.226	8.398
Carbopol 940[5]	non-Newtonian	0.1	-	0.181	23.687
Natrosol 1[6]	non-Newtonian	-	-	0.59	10.8
Natrosol 2[6]	non-Newtonian	-	-	0.75	7

Table 2

Simulation	Liquid	Conc. %	Vessel Geometry	N (rpm)	Re_g
1	Glucose	65	without draft tube	0.880	3
2	Glucose	65	without draft tube	2.940	10
3	Glucose	65	without draft tube	8.814	30
4	Glucose	65	draft tube	0.147	0.5
5	Glucose	65	draft tube	0.880	3
6	Glucose	65	draft tube	2.940	10
7	Glucose	65	draft tube	8.814	30
8	Carbopol 940	0.08	draft tube	4.200	0.175
9	Carbopol 940	0.08	draft tube	6.426	0.373
10	Carbopol 940	0.08	draft tube	12.00	1.128
11	Carbopol 940	0.1	draft tube	11.08	0.322
12	Carbopol 940	0.1	draft tube	21.05	1.073
13	Carbopol 940	0.1	draft tube	31.36	2.135
14	Natrosol 1	-	draft tube	8.688	1
15	Natrosol 1	-	draft tube	18.94	3
16	Natrosol 1	-	draft tube	44.49	10
17	Natrosol 2	-	draft tube	4.788	1
18	Natrosol 2	-	draft tube	11.54	3
19	Natrosol 2	-	draft tube	30.22	10

Table 3

Authors	Np.Re
GLUZ and PAVLUSHENKO (1967)	200
NOVAK and RIEGER (1969)	281
NOVAK and RIEGER (1977)	243
SEICHTER *et al.* (1981)	271
DEAK *et al.* (1985)	391
HIROSE and MURAKAMI (1986)	323
CAUSSANEL (1990)	233
CFD simulation	295

Table 4

Authors	Np.Re
GLUZ and PAVLUSHENKO (1967)	147
NOVAK and RIEGER (1969)	140
DEAK *et al*. (1985)	148
CFD simulation	150

Table 5

Author	Constant k
PROKOPEC and ULBRECHT (1970)	76.87
RIEGER and NOVAK (1973)	16.82 ± 0.87
CFD simulation	16.23

Table 6

Figure 1 : Schematic diagram of the vessel geometry with draft tube.

Figure 2 : CFD representation of the helical screw agitator.

Figure 3 : Effect of grid size on radial profiles of axial velocity at z = 2/5H between the impeller shaft and the draft tube.

Figure 4 : Simulated velocity flow patterns – (a) Simulation 2, (b) Simulation 6 and (c) Simulation 16.

Figure 5 : Simulated velocity flow patterns at 2/5H – (a) Simulation 2, (b) Simulation 6 and (c) Simulation 16.

Figure 6 : Simulated velocity flow patterns – (a) Simulation 2, (b) Simulation 6 and (c) Simulation 16 (i) below the liquid surface and (ii) above the vessel bottom.

Figure 7 : Effect of the rheology and the Reynolds number on the axial velocity.

Figure 8 : Effect of the rheology on axial velocity – a comparison of simulated results with experimental results[5].

Figure 9 : Dependence of the power number on the Reynolds or apparent Reynolds number.

Figure 10 : Power number dependence for the screw agitator with draft tube.

Figure 11 : $Po.Re_g$ dependence for a helical screw agitator with draft tube.

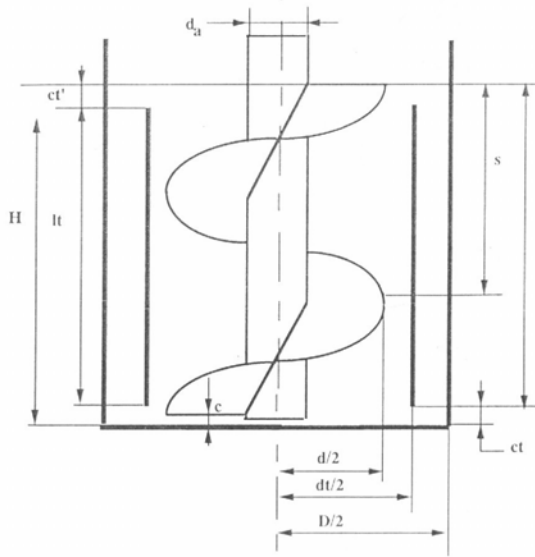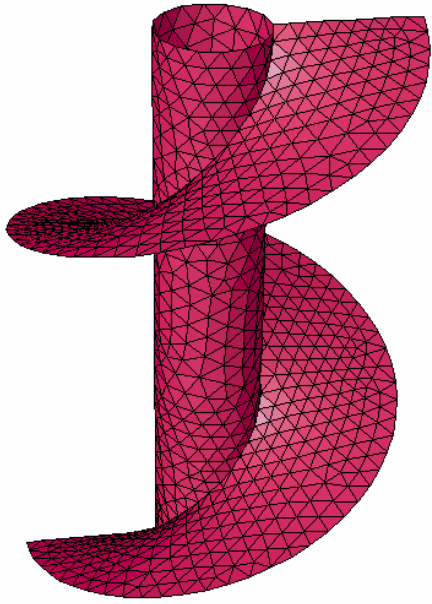**Figure 12 :** Dependence of the circulation number on the Reynolds number.
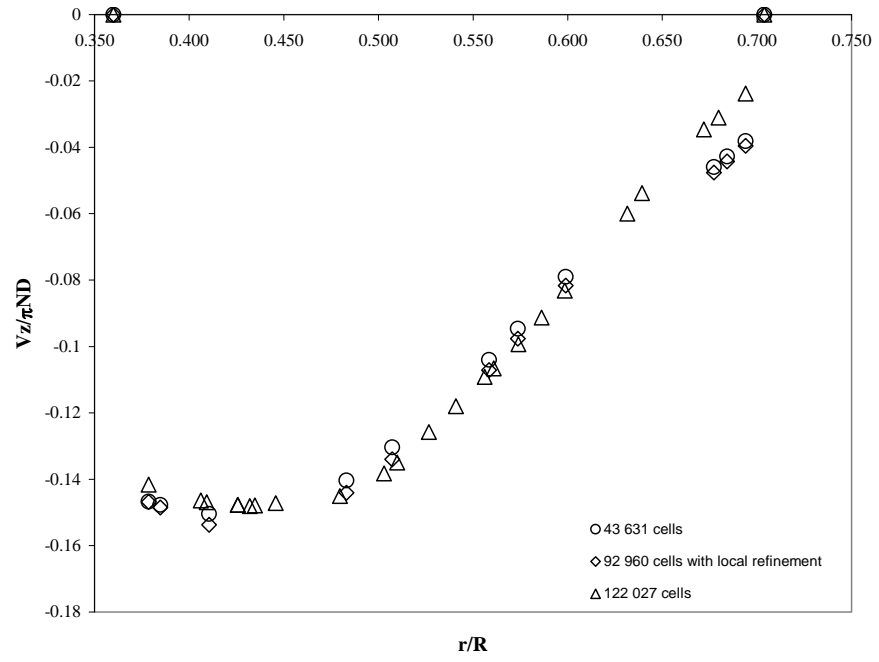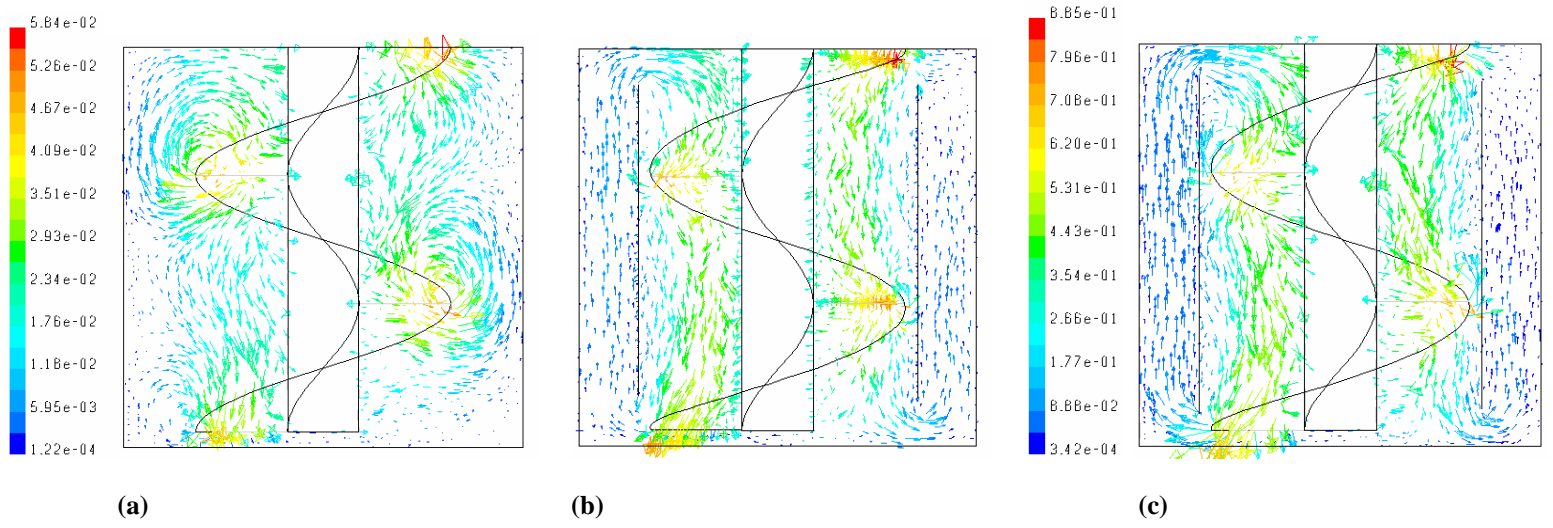
Figure 1

Figure 2

Figure 3

(a)   **(b)**   **(c)**

Figure 4

(a)　　　　　　　　　　**(b)**　　　　　　　　　　**(c)**

Figure 5

(a-i)   (b-i)   (c-i)

(a-ii)   (b-ii)   (c-ii)

Figure 6

Figure 7

Vz/πND

0.080

0.070 ■ This Work n=1

0.060

0.050 ○ Caussanel (1990) n=0.226
● Caussanel (1990) n=1

0.040 □ This Work n=0.226

0.030

0.020

0.010

0.000

0.700   0.750   0.800   0.850   0.900   0.950   1.000

r/R
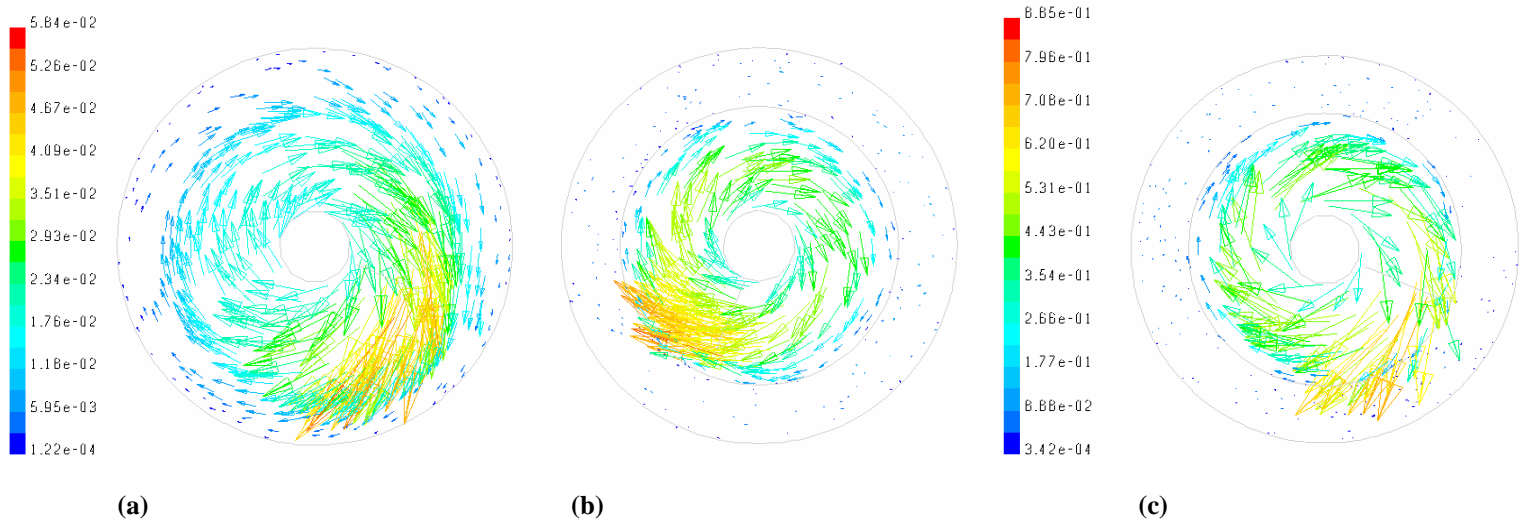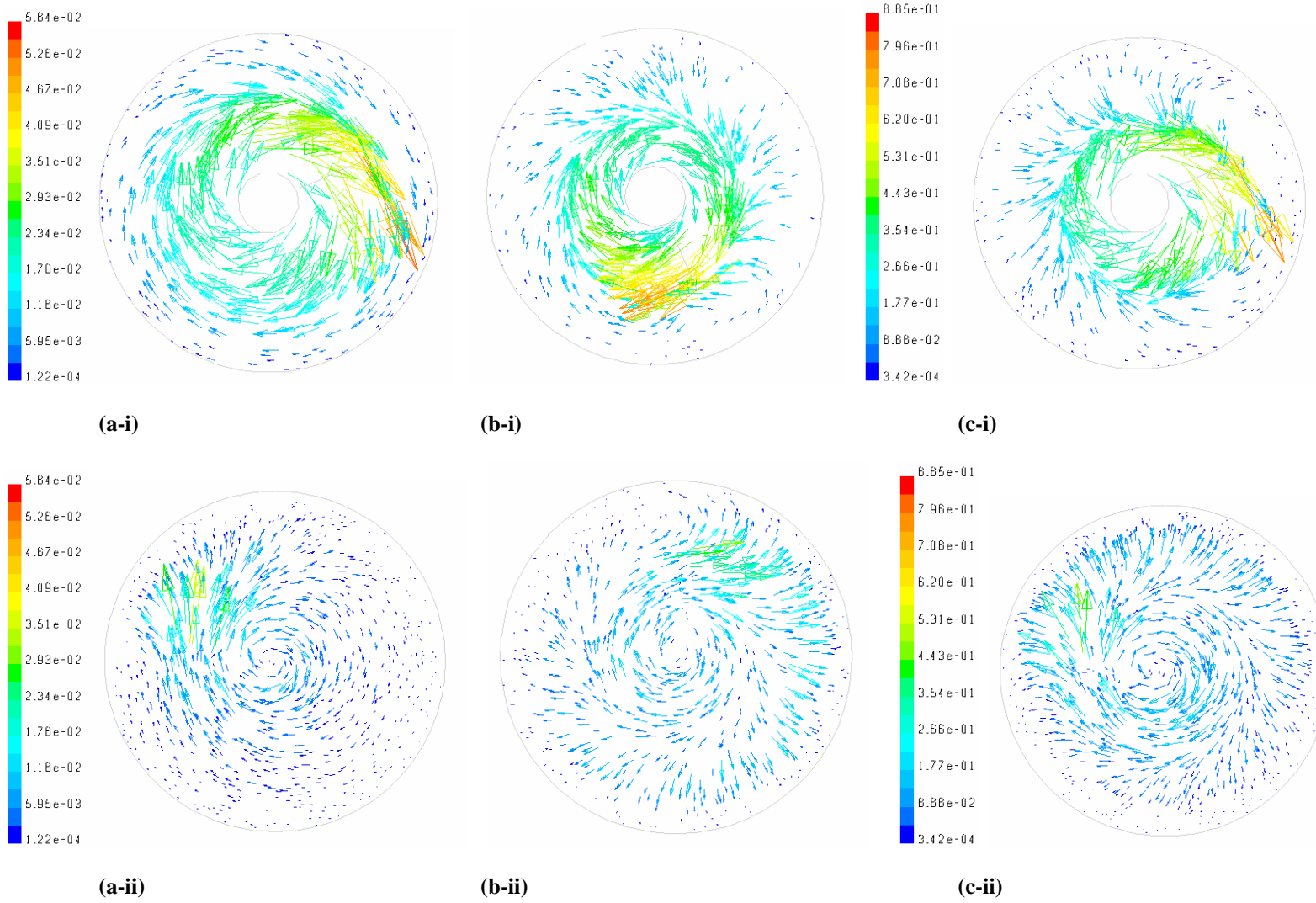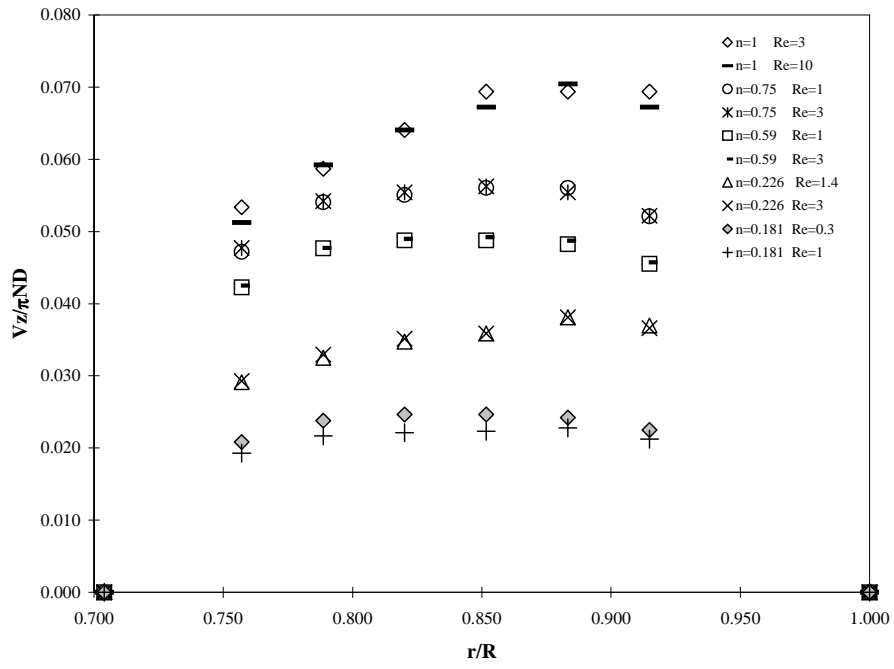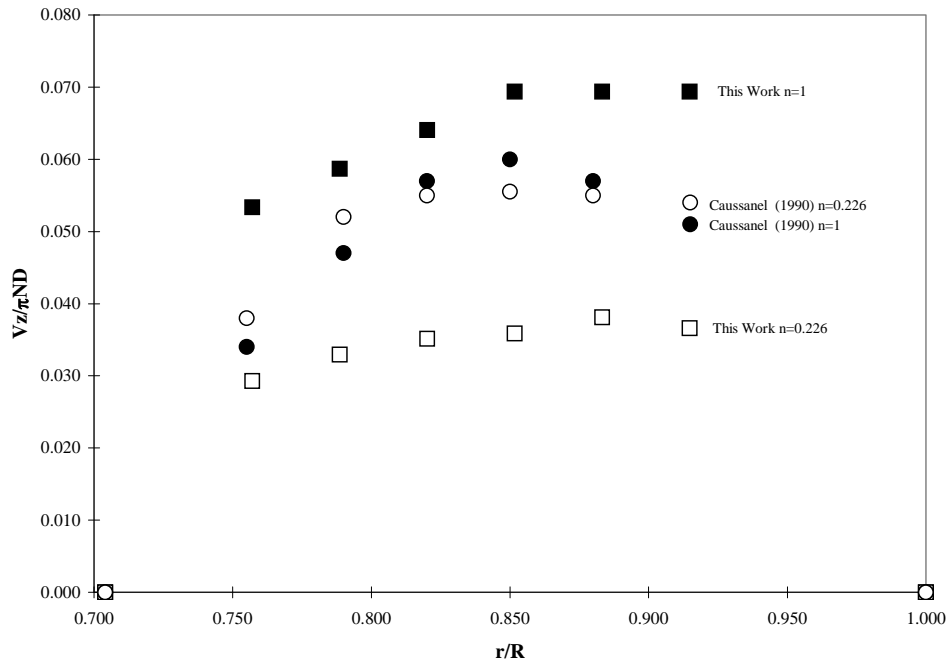
Figure 8

Figure 9

Figure 10

1000

○ 43 631 cells
□ 122 027 cells
△ 92960 cells with local refinement

100

Po.Re$_n$

10

1

0   0.1   0.2   0.3   0.4   0.5   0.6   0.7   0.8   0.9

1-n

Figure 11

Figure showing a plot with axes:

- Y-axis: N_{Qc}, ranging from 0 to 1
- X-axis: Re_g, ranging from 0.1 to 100 (logarithmic)

Legend:
- □ n=1
- ■ n=1 without draft tube
- △ n=0.226
- ▲ n=0.181
- ○ n=0.59
- ● n=0.75

Figure 12